Aerosol Science and Technology 32:369–391 (2000)

Published by Taylor and Francis
0278-6826/00/$12.00 + .00

Modeling and Control of a Titania Aerosol Reactor

Ashish Kalani and Panagiotis D. Christofides
DEPARTMENT OF CHEMICAL ENGINEERING,
UNIVERSITY OF CALIFORNIA,
LOS ANGELES, CA 90095-1592

ABSTRACT. We focus on modeling and control of an aerosol flow reactor used to produce titania powder. We initially present a detailed population balance model for the process which accounts for simultaneous nucleation, Brownian and shear-induced coagulation, and convective transport and describe the spatio-temporal evolution of the aerosol volume distribution. Then, under the assumption of lognormal aerosol volume distribution, the method of moments is employed for the derivation of a model that describes the evolution of the three leading moments of the volume distribution. The moment model, together with the fundamental model that describes the temperature in the reactor and concentrations of the gas-phase species, are subsequently used to synthesize a nonlinear output feedback controller which manipulates the temperature of the reactor wall to achieve an aerosol size distribution in the outlet of the reactor with desired geometric average particle diameter. The nonlinear controller is successfully implemented on the process model and is shown to deal effectively with external disturbances.

INTRODUCTION

Aerosol processes are increasingly being used for the large scale production of nano- and micron-sized particles. These processes have largely replaced other processes which involve multiple steps of wet chemistry, due to the direct gas phase chemical reaction of precursor vapor to form particles and the ease of separation of the particulate products from the gas. Aerosol products, such as TiO_2, B_4C, find widespread use as pigments, reinforcing agents, ceramic powders, optical fibers, carbon blacks, and semiconductor materials. Numerous experimental studies have suggested that aerosol growth occurs in stages, beginning with the gas phase chemical reaction of the reactants to produce monomers or molecules of the condensable species (Friedlander 1977, 1983). The monomers form unstable clusters, which grow further by scavenging smaller clusters and by monomer condensation. Beyond a critical cluster size, nucleation of stable aerosol particles occurs. These particles grow further, mainly by coagulation (condensation and surface reaction are some other growth mechanisms (Pratsinis 1989; Pratsinis and Spicer 1998)). The coagulation rate, which is affected additively by Brownian and shear-induced (turbulent) forces, has a strong effect on particle size and morphology.

Titania powder finds a major use as a white pigment in paints and in absorbants and is commercially produced by two main processes: the gas phase oxidation of titanium tetrachloride, resulting in micron sized particles which are used as white pigments, and the gas phase hydrolysis of titanium tetrachloride, resulting in nano-sized particles which are used as UV absorbants. The pigmentary properties of titania, such as the opacity and gloss, depend largely on the particle size. This fact suggests the design and implementation of advanced model-based feedback control systems on titania aerosol reactors to produce powders with desired size distributions. The development of mathematical models for aerosol reactors that accurately describe the evolution of key variables that characterize the form of the size distribution is usually addressed through application of population balances to the particulate phase (see Akhtar et al. (1991) and Kobata et al. (1991) for modeling of titania aerosol reactors). The population balances are coupled with material and energy balances that describe the rate of change of the state variables of the continuous phase (these are usually systems of nonlinear differential equations which include integrals over the entire particle size spectrum), leading to complete titania process models. The complex nature of population balances has motivated extensive research efforts on the development of numerical methods for the accurate computation of their solution including sectional methods (see, for example, Hounslow et al. (1988), Landgrebe and Pratsinis (1990), Kumar and Ramkrishna (1996a, b), Hill and Ng (1996), and the review paper Ramkrishna (1985)). However, the high complexity of the population balances renders them inappropriate for process simulation and controller design. Fortunately, the fact that most aerosol size distributions can be adequately described by lognormal functions (Williams and Loyalka 1991) allows utilizing the method of moments to derive approximations of the population balances that accurately describe the key properties of the aerosol size distribution; such approximate models are suitable for process simulation and controller design.

In the area of control of processes described by population balance equations, early research focused on stability analysis using Laplace transform and Lyapunov functionals (see, for example, Rawlings and Ray (1987a, b) for such studies in the context of emulsion polymerization reactors) and the application of linear conventional control schemes (e.g., proportional-integral, proportional-integral-derivative, self-tuning control) to crystallizers and emulsion polymerization processes (e.g., Rohani and Bourne (1990), Dimitratos et al. (1994)). These conventional control schemes clearly limit the achievable control quality and may lead to poor performance, or even to destabilization of the closed-loop system, in the presence of severe process nonlinearities. Motivated by this, recent research efforts have focused on the analysis of basic controllability and observability properties of population balance models (Hashemi and Epstein 1982; Semino and Ray 1995), as well as the synthesis and implementation of nonlinear population-balance model based feedback controllers on spatially-homogeneous (Eaton and Rawlings 1990; Chiu and Christofides 1999a, b, 2000) and spatially-inhomogeneous (Kalani and Christofides 1999) particulate processes.

This work focuses on modeling and control of an aerosol flow reactor used to produce titania powder by gas phase oxidation of titanium tetrachloride. Initially, a fundamental mathematical model is derived for the process which describes the spatio-temporal evolution of the three leading moments of the aerosol volume distribution, as well as the evolution of the concentra-

tions of the species and temperature of the continuous phase. The model accounts for simultaneous nucleation, Brownian and turbulent coagulation, and convective transport and comprises of eight nonlinear first-order hyperbolic partial differential equations (PDEs). Then, the process model is used to synthesize a nonlinear output feedback controller which manipulates the temperature of the reactor wall to achieve an aerosol size distribution in the outlet of the reactor with desired geometric average particle diameter. The performance and robustness of the nonlinear controller is successfully tested through computer simulations.

TITANIA PROCESS DESCRIPTION AND MODELING

Process Description

Titania powder is produced under turbulent and nonisothermal conditions in tubular reactors having very short residence times, high temperatures, and relatively low pressures. The premixed and preheated reactants (titanium tetrachloride and oxygen gas) are injected into the reactor where the following exothermic reaction, producing titania monomers and chlorine gas, takes place:

$$TiCl_4(g) + O_2(g) \rightarrow TiO_2(s) + 2Cl_2(g). \tag{1}$$

The size of a single TiO_2 molecule (monomer) is larger than the thermodynamic critical cluster size. As a result, chemical reaction and nucleation become indistinguishable (Pratsinis et al. 1990; Akhtar et al. 1991), thereby implying that the rapid chemical reaction leads to a nucleation burst. The TiO_2 monomers coagulate leading to a larger average particle size and smaller particle concentration. Figure 1 shows a schematic diagram of a typical titania aerosol reactor. In titania aerosol reactors, two forms of coagulation can be distinguished: Brownian coagulation and shear-induced coagulation. Brownian coagulation is the dominant mechanism for particle growth when the particle sizes are small, and may occur as free molecule coagulation when the particle size is comparable to the free mean path of the gas, or as continuum coagulation when the carrier gas can be assumed to be homogeneous compared to the particulate phase. On the other hand, shear-induced coagulation (induced by fluid eddies) becomes dominant when the particle sizes attain macroscopic dimensions. The interplay between Brownian and shear-induced coagulation has a strong effect on the shape of the particle size distribution of the titania product (Pratsinis 1989; Xiong and Pratsinis 1991) and is explicitly taken into account in the mathematical model presented in the next subsection.

Process Model

In this subsection, we present a general model for the titania aerosol process having simultaneous chemical reaction, coagulation, and convective transport. The spatio-temporal evolution of the particle volume distribution in the process can be obtained from a population balance and is described by the following partial integro-differential equation:

$$\begin{aligned}\frac{\partial n}{\partial t} + \frac{\partial (v_z(z,t)n)}{\partial z} - I(v^*)\delta(v - v^*) &= \frac{1}{2}\int_0^v \beta(v-\bar{v},\bar{v},\bar{x})n(v-\bar{v},z,t) \\ &\quad \times n(\bar{v},z,t)\,d\bar{v} \\ &\quad - n(v,z,t)\int_0^\infty \beta(v,\bar{v},\bar{x}) \\ &\quad \times n(\bar{v},z,t)\,d\bar{v},\end{aligned} \tag{2}$$

where $n(v,z,t)$ denotes the TiO_2 particle volume distribution function, v is the particle volume, t is the time, $z \in [0, L]$ is the

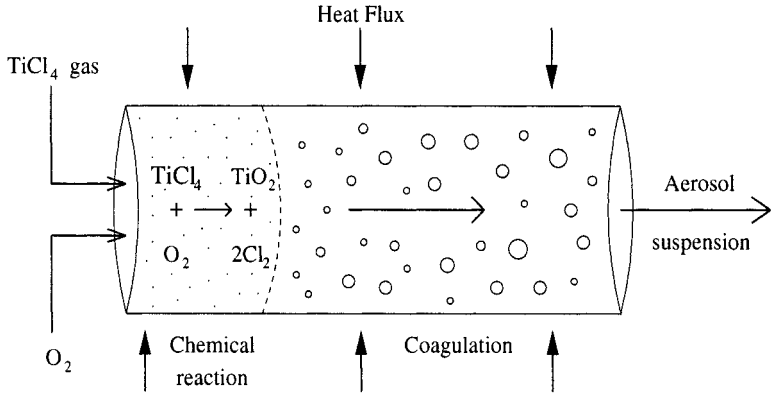

FIGURE 1. A titania aerosol reactor.

spatial coordinate, L is the length of the reactor, $v_z(z,t)$ is the velocity of the fluid in the axial direction, $I(v^*)$ is the nucleation rate, $\beta(v-\overline{v},\overline{v},\overline{x})$ is the coagulation rate, $\delta(\cdot)$ is the standard Dirac function, and $\overline{x}(z,t)$ is an n-dimensional vector of state variables that describe properties of the gas (continuous) phase (e.g., concentrations of O_2 and Cl_2, and temperature of the reactor); the explicit expressions of $v_z(z,t), I(v^*), \beta(v-\overline{v},\overline{v},\overline{x})$ and the equations that describe the variables $\overline{x}$ taken into account in our model are given below.

Referring to the population balance equation of Equation (2), the term $\partial n/\partial t$ describes the rate of change of particle concentration in the particle volume interval $v, v+dv$ and in the spatial interval $z, z+dz$, the term $\partial(v_z(z,t)n)/\partial z$ corresponds to convective transport of aerosol particles, and the term $I(v^*)\delta(v-v^*)$ accounts for the nucleation of particles of critical volume v^* through chemical reaction. Furthermore, the gain and loss of particles by coagulation is described by the terms

$$\frac{1}{2}\int_0^v \beta(v-\overline{v},\overline{v},\overline{x})n(v-\overline{v},z,t)n(\overline{v},z,t)\,d\overline{v}$$

$$\text{and } n(v,z,t)\int_0^\infty \beta(v,\overline{v},\overline{x})\times n(\overline{v},z,t)\,d\overline{v}, \tag{3}$$

respectively. As noted previously, for titania and most other ceramic powders, the nucleation rate is equal to the rate of chemical reaction and the critical volume is the same as the monomer volume. In particular, it has been established (Pratsinis et al. 1990) that the high-temperature oxidation of $TiCl_4$ is a first-order reaction, thereby implying the following expression for the nucleation rate:

$$I(v_1) = N_{av}kC_1, \tag{4}$$

where $k = k_0\exp(-E_{ac}/RT)sec^{-1}$, with $k_0 = 8.26\times10^4 sec^{-1}$ and $E_{ac} = 88.8\ KJmol^{-1}$; N_{av} is the Avogadro's constant ($6.023\times10^{23}\#mol^{-1}$), v_1 is the monomer volume and C_1 is the $TiCl_4$ concentration. On the other hand, the overall collision frequency function, β, is defined as the sum of the Brownian and turbulent shear collision frequency functions (β_B and β_T, respectively):

$$\beta = \beta_B + \beta_T. \tag{5}$$

The Brownian collision frequency function, β_B, has different expressions for the free molecule size and continuum size regimes (Pratsinis 1988). Specifically, in the free

molecule size regime, β_B, takes the form

$$\beta_{FM}(v,\bar{v},\bar{x}) = B_1\left(\frac{1}{v}+\frac{1}{\bar{v}}\right)^{\frac{1}{2}}\left(v^{\frac{1}{3}}+\bar{v}^{\frac{1}{3}}\right)^2, \quad B_1 = (3/4\pi)^{\frac{1}{6}}(6k_BTv_1/m_1)^{\frac{1}{2}}, \tag{6}$$

while, in the continuum size regime, it is given by

$$\beta_C(v,\bar{v},\bar{x}) = B_2\left(\frac{C(v)}{v^{\frac{1}{3}}}+\frac{C(\bar{v})}{\bar{v}^{\frac{1}{3}}}\right) \times \left(v^{\frac{1}{3}}+\bar{v}^{\frac{1}{3}}\right), \; B_2 = \frac{2k_BT}{3\mu}. \tag{7}$$

In Equations (6)–(7), k_B is the Boltzmann's constant ($1.38\times10^{-23}JK^{-1}$), T is the temperature of the gas, μ is the viscosity of the gas, m_1 is the monomer mass, and $C(v)=1+B_3\lambda/r$ is the Cunningham correction factor with r and λ being the particle radius and the mean free path of the gas, respectively, and $B_3=1.257$. The gas mean free path is given by $\lambda=\nu(\pi M_w/2k_BTN_{av})^{\frac{1}{2}}$, where ν is the kinematic viscosity of the gas and M_w is the molecular weight of the gas. The turbulent shear collision frequency function β_T has the following form (Pratsinis 1988):

$$\beta_T(v,\bar{v},\bar{x}) = B_4\left(v^{\frac{1}{3}}+\bar{v}^{\frac{1}{3}}\right)^3, \quad B_4 = 2.3(3/4\pi)(\varepsilon_d/\nu)^{\frac{1}{2}}, \quad \varepsilon_d = 4/D(f/2)^{\frac{3}{2}}v_z^3, \tag{8}$$

where ε_d is the turbulent energy dissipation rate, D is the tube diameter, and f is the Fanning friction factor ($0.0791/Re^{\frac{1}{4}}$) with Re being the Reynolds number.

The spatio-temporal evolution of the concentration of species and temperature of the gas phase can be obtained from mass and energy balances and are described by the following set of equations:

$$\frac{\partial C_i}{\partial t} = -\frac{\partial(v_zC_i)}{\partial z}+\alpha_i kC_i, \quad i=1,\ldots,3,$$
$$\frac{\partial T}{\partial t} = -\frac{\partial(v_zT)}{\partial z} + (kC_1\Delta H + Ua(T_w-T))/C_{pv}, \tag{9}$$

where C_2 and C_3 are O_2 and Cl_2 concentrations, α_1, α_2, and α_3 are -1, -1, and 2, respectively, ΔH is the heat of reaction, U is the overall heat transfer coefficient, a is the heat transfer area per unit volume $(4/D)$, T_w is the wall temperature, and C_{pv} is the volumetric heat capacity of the gas phase. Owing to the rapid and complete consumption of $TiCl_4$ very close to the inlet of the reactor (which is due to the very high reaction rate), the physical properties of the gas phase are calculated under the assumption that it includes only O_2 and Cl_2. Therefore, the viscosity of the gas is calculated from the following reaction (Bird et al. 1960; Kelley 1960):

$$\mu(T) = \sum_{i=1}^{2}\frac{y_ia_i}{y_1\Phi_{i1}+y_2\Phi_{i2}}\sqrt{T}\; kgm^{-1}sec^{-1}, \tag{10}$$

where y_1 and y_2 are the O_2 and Cl_2 mole fractions, respectively, while the volumetric heat capacity of the gas is computed from the following relation (Kelley 1960):

$$C_{pv}(T) = 4.18\sum_{i=1}^{2}C_i\left(d_{i0}+d_{i1}T+\frac{d_{i2}}{T^2}\right) Jm^{-3}K^{-1}. \tag{11}$$

The values of the parameters used in Equation (10)–(11) are given in Table 1.

The fluid flow is assumed to be choked once the gas velocity reaches the acoustic limit. The pressure drop occurring due to frictional losses at the wall (there is no change in the number of moles in the gas phase due to chemical reaction) is modeled as (Xiong and Pratsinis 1991)

$$\frac{\partial P}{\partial z} = -2f\rho v_z^2/D, \quad v_z < v_{z,sn}, \quad = -2f\rho v_{z,sn}^2/D, \quad v_z \geq v_{z,sn}, \tag{12}$$

TABLE 1. Parameters used in Equations (10)–(11).

a_1	1.73×10^{-6}
a_2	1.46×10^{-6}
Φ_{11}	1.0
Φ_{12}	1.59
Φ_{21}	0.605
Φ_{22}	1.0
d_{10}	7.16
d_{11}	10^{-3}
d_{12}	-4.0×10^{4}
d_{20}	8.85
d_{21}	1.6×10^{-4}
d_{22}	-6.8×10^{4}

where P is the pressure, ρ is the gas density, and $v_{z,sn}$ is the sonic velocity in the gas medium at a given temperature and is equal to $(\gamma RT/M_w)^{\frac{1}{2}}$, with γ and R being the heat capacity ratio (1.4) and the universal gas constant $(8.314 Jmol^{-1}K^{-1})$, respectively. Therefore, the equation which describes the velocity profile, $v_z(z,t)$, when $v_z < v_{z,sn}$, takes the form

$$\frac{\partial v_z}{\partial t} = -v_z \frac{\partial v_z}{\partial z} + 2fv_z^2/D. \qquad (13)$$

REMARK 1: Some remarks need to be made for Equations (2) and (9): a) the spatial differential operators are nonlinear due to the nonlinearity in the flux terms (i.e., the velocity profile is not constant and changes with time and space according to Equation (13); b) diffusive and dispersive effects in the axial and radial directions are neglected; c) particle deposition on the tube walls is neglected; and d) the coalescence between two colliding particles is assumed to be instantaneous.

REMARK 2: In Equation (6), the expansion of the expression for β_{FM} yields a very large number of terms which are necessary for covering a wide range of the particle volumes; this adds significant complexity to the numerical simulation of the process model. To circumvent this computational problem, the following approximation, proposed in (Lee et al. 1984), was used in our numerical calculations described in the following sections:

$$\left(\frac{1}{v} + \frac{1}{\overline{v}}\right)^{\frac{1}{2}} = b\left(\frac{1}{v^{\frac{1}{2}}} + \frac{1}{\overline{v}^{\frac{1}{2}}}\right), \qquad (14)$$

where the coefficient b depends on the geometric standard deviation and moments of the particle volume distribution.

REMARK 3: In Equation (2), it has been assumed that there is instantaneous coalescence between the colliding particles. However, below a temperature of about 1500 K, the coalescence rate becomes comparable to or slower than the coagulation rate and the above assumption no longer holds (Xiong and Pratsinis 1991). Colliding particles fail to fuse (or coalesce), causing further growth by particle collision to be negligible. Therefore, following the development in (Xiong and Pratsinis 1991), we assume that the coagulation rate below 1500 K is 0.

LOGNORMAL AEROSOL MOMENT MODEL

The complexity of the population balance model (partial integro-differential equation) of Equation (2) does not allow its direct use for numerical computation of the size distribution in real-time (a direct discretization of this model through finite-differences or sectional method leads to thousands of ordinary differential equations), as well as for the synthesis of feedback controllers that can be readily implemented in practice. Motivated by the need to circumvent these problems and the experimental observation that titania aerosol volume distributions can be adequately characterized by lognormal (self-preserving) functions, we initially apply the method of moments to Equation (2) to compute approximate models that describe the spa-

tio-temporal evolution of the three leading moments of the volume distribution in the free molecule size, continuum size, and turbulent shear regimes. Then, under the assumption of lognormal volume distribution, we compute the moment model that describes aerosol dynamics over the entire particle volume spectrum. This approach is based on the fact that moment models provide adequate simplification of the population balance equation by modeling the key average bulk properties of the evolving product.

Moment Model

In this subsection, the PDEs describing the spatio-temporal evolution of the three leading moments (i.e., the zeroth, first, and second moments) of the volume distribution for the free molecule size, continuum size, and turbulent shear regimes are presented. To this end, we define the kth moment as the particle volume weighted integral of the particle number density function:

$$M_k(z,t) = \int_0^\infty v^k n(v,z,t)\,dv. \tag{15}$$

The computation of the moment equations is done by substituting the appropriate expressions for the nucleation and coagulation rates into Equation (2), multiplying by v^k, and integrating over all particle volumes. The detailed derivation of some of the moment equations given below is described in the appendix.

We begin with the presentation of the PDE that describes the evolution of the first moment, M_1, which physically corresponds to the aerosol volume. Since the aerosol volume is independent of the coagulation rate and depends only on the nucleation rate, the PDE that describes the evolution of M_1 is the same for all three regimes and has the following form:

$$\frac{\partial M_1}{\partial t} = -\frac{\partial (v_z M_1)}{\partial z} + N_{av} k C_1 v_1. \tag{16}$$

Free molecule size regime. Substituting $\beta = \beta_{FM}$ into Equation (2) and integrating over all particle volumes, the spatio-temporal evolution of the zeroth moment, M_0, which represents the aerosol concentration and is affected by nucleation and coagulation, is given by

$$\frac{\partial M_0}{\partial t} = -\frac{\partial (v_z M_0)}{\partial z} + N_{av} k C_1 - b_0 B_1 (M_{2/3} M_{-1/2} + 2 M_{1/3} M_{-1/6} + M_{1/6} M_0), \tag{17}$$

where the coefficient b_0 is used as b in Equation (14) and is calculated for the zeroth moment. On the other hand, the evolution of the second moment, M_2, which depends both on nucleation and coagulation, is described by

$$\frac{\partial M_2}{\partial t} = -\frac{\partial (v_z M_2)}{\partial z} + N_{av} k C_1 v_1^2 + 2 b_2 B_1 (M_{5/3} M_{1/2} + 2 M_{4/3} M_{5/6} + M_{7/6} M_1), \tag{18}$$

where b_2 is used as b_0 but for the coagulation kernel of the second moment.

Continuum size regime. Similar to the case of the free molecule regime, the PDEs that describe the spatio-temporal evolution of the zeroth and second moments of the aerosol volume distribution in the continuum size regime can be obtained by setting $\beta = \beta_C$ in Equation (2), multiplying by v^k (k is equal to 0 and 2, respectively), and integrating over all particle volumes. The

resulting PDEs have the following form:

$$\frac{\partial M_0}{\partial t} = -\frac{\partial (v_z M_0)}{\partial z} + N_{av} k C_1 - B_2 \Big[M_0^2 + M_{1/3} M_{-1/3} + B_3 \lambda (4\pi/3)^{\frac{1}{3}} (M_0 M_{-1/3} + M_{1/3} M_{-2/3}) \Big], \quad (19)$$

$$\frac{\partial M_2}{\partial t} = -\frac{\partial (v_z M_2)}{\partial z} + N_{av} k C_1 v_1^2 + 2B_2 \Big[M_1^2 + M_{4/3} M_{2/3} + B_3 \lambda (4\pi/3)^{\frac{1}{3}} (M_1 M_{2/3} + M_{1/3} M_{4/3}) \Big]. \quad (20)$$

Turbulent shear regime. Finally, following the same approach as in the free molecule and continuum size regimes, we obtain the following PDEs that describe the spatio-temporal evolution of the zeroth and second moments of the aerosol volume distribution in the turbulent shear regime:

$$\frac{\partial M_0}{\partial t} = -\frac{\partial (v_z M_0)}{\partial z} + N_{av} k C_1 - B_4 (M_0 M_1 + 3 M_{1/3} M_{2/3}), \quad (21)$$

$$\frac{\partial M_2}{\partial t} = -\frac{\partial (v_z M_2)}{\partial z} + N_{av} k C_1 v_1^2 + 2B_4 (M_1 M_2 + 3 M_{4/3} M_{5/3}). \quad (22)$$

Lognormal Particle Volume Distribution

Studies suggest that the volume distributions of many aerosol products including titania can be adequately approximated by unimodal lognormal functions. In addition, the variables included in lognormal functions, like the geometric average particle volume, are frequently used in industry to characterize aerosol products. Therefore, it is meaningful to represent titania aerosol volume distributions by lognormal functions. Specifically, titania aerosols can be adequately approximated by unimodal lognormal functions of the form (Xiong and Pratsinis 1991):

$$n(v, z, t) = \frac{1}{3\sqrt{2\pi} \ln \sigma} \exp\left(-\frac{ln^2 (v/v_g)}{18 ln^2 \sigma} \right) \frac{1}{v}, \quad (23)$$

where v_g is the geometric average particle volume and σ is the standard deviation. v_g and σ can be expressed in terms of the first three moments of the distribution according to the following relations (Brock et al. 1986):

$$v_g = \frac{M_1^2}{M_0^{\frac{3}{2}} M_2^{\frac{1}{2}}}, \; ln^2 \sigma = \frac{1}{9} ln \left(\frac{M_0 M_2}{M_1^2} \right). \quad (24)$$

Furthermore, the moment description of the system can be closed according to the following relation:

$$M_k = M_0 v_g^k \exp\left(\frac{9}{2} k^2 ln^2 \sigma \right). \quad (25)$$

From Equations (23)–(24), it is clear that lognormal aerosols can be accurately described in terms of the three leading moments of the volume distribution. Therefore, volume distributions of lognormal aerosols can be exactly obtained by simulating the moment model that describes the spatio-temporal evolution of the three leading moments of the distribution over the entire particle volume spectrum. Such a moment model can be obtained as follows. First, the higher-order and fractional moments in Equations (16)–(22) are expressed in terms of the zeroth, first, and second moments through the use of Equations (24)–(25). Then, the zeroth and second moment equations for the free molecule size and continuum size regimes are combined to describe the aerosol dynamics over the entire particle volume spectrum by using

the harmonic average of the dimensionless coagulation rates in the free molecule size and continuum size regimes (the dimensionless harmonic average coagulation rate reduces to the appropriate limits in the two limiting size regimes and closely approximates the Fuchs-Sutugin approximation in the transition regime (Pratsinis 1988). Finally, by adding the dimensionless turbulent (shear-induced) coagulation rate to the dimensionless harmonic mean Brownian coagulation rate, the following PDE system that describes the evolution of the three leading moments of the titania aerosol volume distribution over the entire particle volume spectrum is obtained (see Table 2 for the list of dimensionless variables).

Zeroth moment:

$$\frac{\partial N}{\partial \theta} = -\phi \frac{\partial(\overline{v}_z N)}{\partial \overline{z}} + k' x_1 - \xi N^2, \qquad (26)$$

where

$$\xi = \frac{\xi_{FM}\,\xi_C}{\xi_{FM} + \xi_C} + \xi_T,$$

$$\xi_{FM} = b_0 r_g'^{\frac{1}{2}} \overline{T}^{\frac{1}{2}} \left[\exp\left(\frac{25}{8} ln^2\sigma\right) + 2\exp\left(\frac{5}{8} ln^2\sigma\right) + \exp\left(\frac{1}{8} ln^2\sigma\right) \right],$$

$$\xi_C = K_1 \psi^{-1} \overline{T} \left[1 + \exp(ln^2\sigma) + B_3(K_{n_1}/r_g')\exp(0.5 ln^2\sigma) \times (1 + \exp(2 ln^2\sigma)) \right], \qquad (27)$$

$$\xi_T = K_2 \eta\, v_g' \exp\left(\frac{9}{2} ln^2\sigma\right) \times [1 + 3\exp(-2 ln^2\sigma)].$$

First moment:

$$\frac{\partial V}{\partial \theta} = -\phi \frac{\partial(\overline{v}_z V)}{\partial \overline{z}} + k' x_1. \qquad (28)$$

TABLE 2. Dimensionless variables for the model of Equations (26)–(30).

$N = M_0 / C_0 N_{av}$	Aerosol number concentration
$V = M_1 / C_0 N_{av} v_1$	Aerosol volume concentration
$V_2 = M_2 / C_0 N_{av} v_1^2$	Second aerosol moment
$\tau_{fm}(T) = (6 k_B T r_1 v_1 / m_1)^{-\frac{1}{2}} / C_0 N_{av}$	Characteristic time for particle growth in free molecule regime
$\tau_c(T) = 3\mu / 2 k_B T C_0 N_{av}$	Characteristic time for particle growth in continuum regime
$\tau_{sf}(T) = 4\pi(\varepsilon_d/\nu)^{-\frac{1}{2}} / 6.9 v_1 C_0 N_{av}$	Characteristic time for particle growth by shear forces
$\tau_r(T) = 1/k_0 \exp(-E_{ac}/RT)$	Characteristic time for chemical reaction
$K_{n1} = \lambda / r_1$	Monomer Knudsen number
$\tau_{fm,o} = \tau_{fm}(T_0)$	
$\tau_{c,o} = \tau_c(T_0)$	
$\tau_{sf,o} = \tau_{sf}(T_0)$	
$\tau_{r,o} = \tau_r(T_0)$	
$k' = \tau / \tau_{r,o}$	
$K_1 = \tau_{fm,o} / \tau_{c,o}$	
$K_2 = \tau_{fm,o} / \tau_{sf,o}$	
$\psi = \mu / \mu_o$	
$\eta = (\varepsilon_d/\nu)^{\frac{1}{2}} (\varepsilon_{d,o}/\nu_o)^{-\frac{1}{2}}$	
$v_g' = v_g / v_1$	
$r_g' = r_g / r_1$	
$\overline{z} = z / L$	
$\overline{v}_z = v_z / v_{z,o}$	
$\phi = v_{z,o} \tau_{fm,o} / L$	
$\theta = t / \tau_{fm,o}$	

Second moment:

$$\frac{\partial V_2}{\partial \theta} = -\phi \frac{\partial(\overline{v}_z V_2)}{\partial \overline{z}} + k' x_1 + 2\zeta V^2, \quad (29)$$

where

$$\zeta = \frac{\zeta_{FM}\zeta_C}{\zeta_{FM}+\zeta_C} + \zeta_T,$$

$$\zeta_{FM} = b_2 r_g'^{\frac{1}{2}} \overline{T}^{\frac{1}{2}} \exp\left(\frac{3}{2} ln^2\sigma\right)\left[\exp\left(\frac{25}{8} ln^2\sigma\right) + 2\exp\left(\frac{5}{8} ln^2\sigma\right) + \exp\left(\frac{1}{8} ln^2\sigma\right)\right],$$

$$\zeta_C = K_1 \psi^{-1} \overline{T}\left[1 + \exp(ln^2\sigma) + B_3(K_{n_1}/r_g')\exp(-0.5 ln^2\sigma) \times (1+\exp(-2 ln^2\sigma))\right], \quad (30)$$

$$\zeta_T = \exp(9 ln^2\sigma)\xi_T.$$

Finally, the model of the titania aerosol reactor is completed by deriving the dimensionless PDEs, which describe the spatio-temporal evolution of the concentration of the species, and the temperature and fluid-dynamics of the gas phase (see Tables 2, 3, and 4 for the list of dimensionless variables and physical and process parameters):

$$\frac{\partial \overline{C}_i}{\partial \theta} = -\phi \frac{\partial\left(\overline{v}_z \overline{C}_i\right)}{\partial \overline{z}} + \alpha_i k' \overline{C}_i, \quad i = 1,\ldots,3, \quad (31)$$

$$\frac{\partial \overline{T}}{\partial \theta} = -\phi \frac{\partial\left(\overline{v}_z \overline{T}\right)}{\partial \overline{z}} + \left[A k' \overline{C}_1 + B\left(\overline{T}_w - \overline{T}\right)\right]\overline{C}_{pv}^{-1}, \quad (32)$$

$$\frac{\partial \overline{v}_z}{\partial \theta} = -\phi \overline{v}_z \frac{\partial \overline{v}_z}{\partial \overline{z}} + E\overline{v}_z^2. \quad (33)$$

REMARK 4: In Equations (27) and (30), $b_0 = 0.633 + 0.092\sigma^2 - 0.022\sigma^3$ and $b_2 = 0.39 + 0.5\sigma - 0.214\sigma^2 + 0.029\sigma^3$, respectively. These polynomial expressions are obtained as functions of σ by regression (Pratsinis 1988).

TABLE 3. Process model parameters for the simulation study.

$L = 125\ m$	Reactor length
$D = 0.25\ m$	Reactor diameter
$Re = 5 \times 10^5$	Reynolds number
$P_o = 4\ atm$	Inlet pressure
$T_o = 2000 K$	Inlet temperature
$y_{1o} = 0.4$	Inlet $TiCl_4$ molar fraction
$v_{z,o} = 87.2\ msec^{-1}$	Inlet velocity of process fluid
$C_0 = 24.37\ molm^{-3}$	Inlet concentration of process fluid
$U = 160\ Jm^{-2}s^{-1}K^{-1}$	Overall heat transfer coefficient
$\Delta H_R = 88\ KJmol^{-1}$	Heat of reaction
$C_{pv,o} = 1615.25\ Jm^{-3}K^{-1}$	Inlet volumetric heat capacity of process fluid
$\mu_o = 6.7 \times 10^{-5}\ kgm^{-1}s^{-1}$	Inlet viscosity of process fluid
$v_1 = 3.12 \times 10^{-29}\ m^3$	Monomer volume

TABLE 4. Dimensionless variables for the model of Equations (31)–(33).

$C_{pv} = C_{pv}/C_{pv,o}$
$A = C_0 \Delta H / C_{pv,o} T_0$
$B = Ua\tau_{fm,o}/C_{pv,o}$
$E = 2f\tau_{fm,o}\overline{v}_{z,o}/D$
$\overline{C}_i = C_i/C_0$
$\overline{T} = T/T_0$
$\overline{T}_w = T_w/T_0$

Analysis of the Open-Loop System

In this subsection, we perform several simulation runs of the open-loop (uncontrolled) process which allows us to obtain key insights into the interplay of the various coagulation mechanisms taking place in the process and the formulation of a meaningful control configuration (i.e., selection of manipulated variable and measurements). The process model of Equations

(26), (28), (29), (31)–(33) was numerically solved by using the method of finite-differences for spatial discretization (the spatial interval was discretized into 200 equispaced subintervals), the computation of the integrals over the entire particle volume spectrum was done by using Wilson's method, and the time-integration was accomplished by using a standard 4th-order Runge-Kutta algorithm. We established through numerous simulations that the result obtained with this discretization scheme are accurate in the sense that further increase in the number of discretization intervals yields almost identical results.

Figure 2 displays the steady-state profile of the geometric standard deviation of the particle volume distribution versus the geometric average particle diameter along the axis of the reactor. As discussed previously, the nucleation burst at the beginning of the reactor causes a sudden increase in σ. However, with the rapid completion of the chemical reaction, σ begins to decrease and approaches its asymptotic value under Brownian coagulation (about 1.4). Towards the end of the reactor, shear-induced coagulation becomes important due to the increasing average particle size and extends the higher end of the size distribution, thus causing σ to increase again (Pratsinis 1989). In this work, the residence time in the reactor is chosen so that the geometric average particle diameter of the aerosol product is the one corresponding to the smallest powder polydispersity.

On the other hand, since the control objective in titania aerosol reactor is to produce titania powder with desired size distribution, we also studied the effect of the wall temperature on the geometric average particle diameter; a variable that is typically used in industry to characterize and compare different aerosol size distributions. Understanding of this effect could lead to a formulation of a meaningful con-

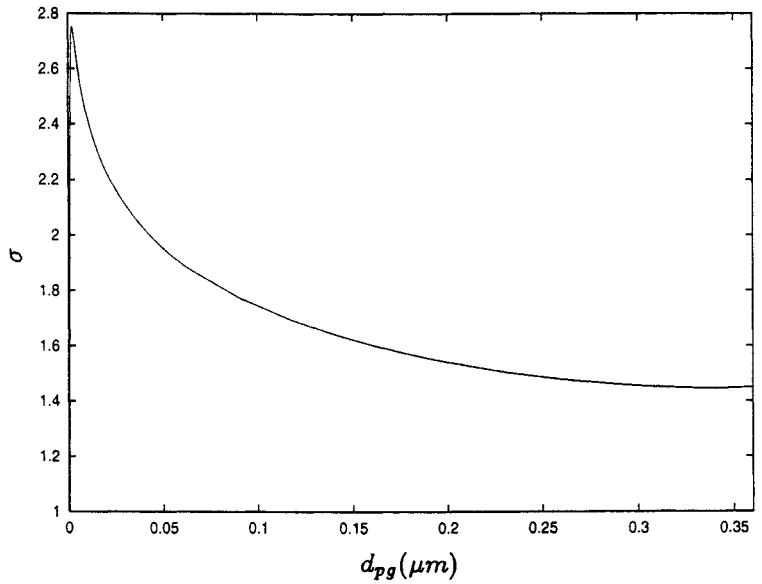

FIGURE 2. Steady-state profile of σ versus d_{pg} (μm).

trol problem. Figure 3 gives the plots of the geometric average particle diameter, d_{pg}, with two different values of the wall temperature, $2000K$ and $2400K$. It was assumed that the coagulation rate below $1500K$ is negligible (Xiong and Pratsinis 1991), hence, there was no increase in d_{pg} in the middle part of the reactor where the process temperature drops below $1500K$ due to Joule cooling. From these results, it is clear that the wall temperature is a variable that has a very significant effect on the geometric average particle diameter, and therefore it is a meaningful choice for manipulated input (see subsection Closed-Loop Simulations below for results of the closed-loop system).

Finally, in order to simplify the presentation of the controller synthesis results in the next section, we rewrite the process model in a vector form. Defining a new vector of state variables $x = [N\ V\ V_2\ \overline{C}_i\ \overline{C}_2\ \overline{C}_3\ \overline{T}\ \overline{v}_z]$, the PDE system of Equations (26), (28), (29), (31)–(33) can be written in the following general form:

$$\frac{\partial x}{\partial \theta} = A(x)\frac{\partial x}{\partial \overline{z}} + f(x) + g(x)b(\overline{z})u(\theta), \tag{34}$$

where $A(x)$ is a matrix which includes elements that may be nonlinear functions of x, $f(x)$, $g(x)$ are nonlinear vector functions, $u(\theta)$ is the manipulated input (wall temperature), and $b(\overline{z})$ is a function that determines how the control action is distributed in space. The specific form of the matrix $A(x)$ and the nonlinear vector functions $f(x)$, $g(x)$ is omitted due to space limitations. The system of Equation (34) will be used for controller design in the next section.

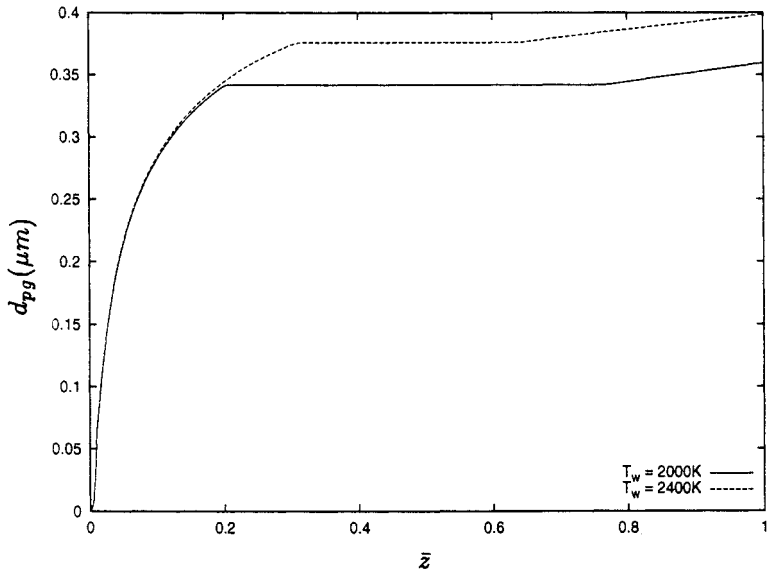

FIGURE 3. Steady-state profile of d_{pg} (μm) for two different wall temperature values.

NONLINEAR CONTROL

Controller Synthesis

In this subsection, we discuss the theoretical results needed to synthesize nonlinear output feedback controllers for titania aerosol reactors that attain size distributions with desired characteristics on the basis of PDE models of the form of Equation (34). The reader may refer to (Christofides and Daoutidis 1996) for details and explanations of the various concepts and results presented below. Owing to the hyperbolic nature of the PDE model of Equation (34), the eigenvalues of the corresponding spatial differential operator cluster along vertical or nearly vertical asymptotes in the complex plane, which implies that an infinite number of eigenmodes is required to accurately describe the dynamic behavior of the PDE. This property does not allow deriving low-order approximations of the PDE model of Equation (34) using modal decomposition techniques and suggests addressing the control problem directly on the basis of the PDE system.

We initially define a general controlled output, $y(\theta)$, as

$$y(\theta) = \int_0^1 c(\bar{z}) h(x(\bar{z}, \theta)) d\bar{z} \equiv Ch(x), \tag{35}$$

where $h(x(\bar{z}, \theta))$ is a nonlinear function of the state of the process (this allows considering controlled outputs that depend in a nonlinear fashion on x, e.g., d_{pg}), $c(\bar{z})$ is a smooth known function which depends on the desired control objective (for example, regulation of d_{pg} in the outlet of the aerosol reactor requires $c(\bar{z}) = \delta(\bar{z} - 1)$), and C is an integral operator. The definition of controlled output allows introducing the concept of characteristic index between the output y and the manipulated input u which will be used in the synthesis of the controller. More specifically, referring to the system of Equation (34), the characteristic index of y with respect to u is the smallest integer $\bar{\sigma}$ for which (Christofides and Daoutidis 1996)

$$CL_g \left(\sum_{j=1}^{n} \frac{\partial x_j}{\partial \bar{z}} L_{a_j} + L_f \right)^{\bar{\sigma}-1} h(x) b(\bar{z}) \quad 0, \tag{36}$$

where a_j denotes the jth column vector of the matrix $A(x)$ and L_{a_j}, L_f denote the standard Lie derivative notation ($L_f h(x) = (\partial h / \partial x) f(x)$). From the above definition, it follows that $\bar{\sigma}$ depends on the structure of the process (matrix $A(x)$ and functions $f(x), g(x), h(x)$), as well as on the actuator and performance specification functions, $b(\bar{z})$ and $c(\bar{z})$, respectively.

The state feedback control problem is formulated as the one of synthesizing distributed controllers of the general form

$$u = S(x) + s(x) y_{sp}, \tag{37}$$

where $S(x)$ is a smooth nonlinear operator, $s(x)$ is an invertible matrix of smooth functionals, and y_{sp} is the set-point that stabilize the closed-loop system and force the following linear input/output response:

$$\gamma_{\bar{\sigma}} \frac{d^{\bar{\sigma}} y}{d\theta^{\bar{\sigma}}} + \cdots + \gamma_1 \frac{dy}{d\theta} + y = y_{sp}, \tag{38}$$

where $\gamma_1, \gamma_2 \cdots, \gamma_{\bar{\sigma}}$ are adjustable parameters, which have to be chosen so that the roots of the polynomial $\gamma_{\bar{\sigma}} s^{\bar{\sigma}} + \gamma_{\bar{\sigma}-1} s^{\bar{\sigma}-1} + \cdots + \gamma_1 s + 1 = 0$ lie in the left-half of the complex plane in order to guarantee stability of the input/output dynamics of the closed-loop system.

This controller synthesis problem leads to the following nonlinear distributed state feedback controller (Christofides and

Daoutidis 1996):

$$u = \left[C\gamma_{\bar{\sigma}} L_g \left(\sum_{j=1}^{n} \frac{\partial x_j}{\partial \bar{z}} L_{a_j} + L_f \right)^{\bar{\sigma}-1} \times h(x) b(\bar{z}) \right]^{-1} \left\{ y_{sp} - Ch(x) - \sum_{v=1}^{\bar{\sigma}} C\gamma_v \left(\sum_{j=1}^{n} \frac{\partial x_j}{\partial \bar{z}} L_{a_j} + L_f \right)^{v} h(x) \right\}, \tag{39}$$

which enforces stability and the response of Equation (38) in the closed-loop system of Equations (34)–(39), provided that the system of Equation (34) is minimum-phase (this property is needed to ensure stability of the internal dynamics of the closed-loop system and is satisfied by the titania aerosol reactor; see next subsection).

The implementation of the distributed nonlinear controller of Equation (39) requires knowledge of the state $x(z,t)$ at all positions and times, which may not be available in some practical applications. To overcome this problem, we use the following state observer to estimate the state $x(z,t)$ of the system of Equation (34) in space and time:

$$\frac{\partial w}{\partial \theta} = A(w)\frac{\partial w}{\partial \bar{z}} + f(w) + g(w)b(z)u + P(y - Ch(w)), \tag{40}$$

where w denotes the observer state vector and P is a linear operator, designed on the basis of the linearization of the system of Equation (40) so that the system of Equation (40) is exponentially stable (see Christofides and Daoutidis (1996) for details). The combination of the state feedback controller of Equation (39) with the state observer of Equation (40) leads to a nonlinear output feedback controller of the form

$$\begin{aligned} \frac{\partial w}{\partial \theta} = {} & A(w)\frac{\partial w}{\partial \bar{z}} + f(w) \\ & + g(w)b(\bar{z}) \left[\gamma_{\bar{\sigma}} C L_g \times \left(\sum_{j=1}^{n} \frac{\partial w_j}{\partial \bar{z}} L_{a_j} + L_f \right)^{\bar{\sigma}-1} \times h(w) b(\bar{z}) \right]^{-1} \\ & \times \left\{ y_{sp} - Ch(w) - \sum_{v=1}^{\bar{\sigma}} \gamma_v C \left(\sum_{j=1}^{n} \frac{\partial w_j}{\partial \bar{z}} L_{a_j} + L_f \right)^{v} h(w) \right\} \\ & + P(y - Ch(w)), \end{aligned} \tag{41}$$

$$u = \left[\gamma_{\bar{\sigma}} C L_g \left(\sum_{j=1}^{n} \frac{\partial w_j}{\partial \bar{z}} L_{a_j} + L_f \right)^{\bar{\sigma}-1} \times h(w) b(\bar{z}) \right]^{-1} \left\{ y_{sp} - Ch(w) - \sum_{v=1}^{\bar{\sigma}} \gamma_v C \left(\sum_{j=1}^{n} \frac{\partial w_j}{\partial \bar{z}} L_{a_j} + L_f \right)^{v} h(w) \right\}$$

that enforces stability and the input/output response of Equation (38) in the closed-loop system. As expected, the implementation of the output feedback controller of Equation (41) requires algebraic manipulations as well as differentiations and integrations in space.

REMARK 5: Note that in the case of imperfect initialization of the observer states (i.e., $w(\bar{z},0) \neq x(\bar{z},0)$), although a slight deterioration of the performance may occur (i.e., the input/output response of Equation (38) will not be exactly imposed in the closed-loop system), the distributed output feedback controller of Equation (41) guarantees

exponential stability and asymptotic output tracking in the closed-loop system. Furthermore, in the case of open-loop stable processes, the integral gain of the observer, P, can be set identically equal to 0, in which case the rate of convergence of the estimates, $w(\bar{z}, \theta)$, to the true values, $x(\bar{z}, \theta)$, depends on the location of the stable poles of the open-loop process.

REMARK 6: The local exponential stability of the closed-loop system under the controller of Equation (41) guarantees robustness (i.e., boundedness of the state of the closed-loop system) with respect to sufficiently small external disturbances and uncertainty in the process parameters. Furthermore, it is possible to implement a linear error feedback controller (for example, a proportional integral (PI) controller) around the $(y - y_{sp})$ loop to ensure asymptotic offsetless output tracking in the closed-loop system, in the presence of disturbances and model uncertainty.

REMARK 7: It can be shown using singular perturbation techniques that the controller of Equation (41) possesses a robustness property with respect to unmodeled dynamics provided that they are asymptotically stable and sufficiently fast (i.e., the controller enforces exponential stability and output tracking despite the presence of additional dynamics in the process). This robustness property is of significant practical importance because unmodeled dynamics occur frequently in practice due to actuator and sensor dynamics, as well as other fast process dynamics.

Closed-Loop Simulations

Motivated by the results of the simulations presented in subsection Analysis of the Open-Loop System, the control problem was formulated as the one of controlling the geometric average particle diameter in the outlet of the reactor by manipulating the wall temperature, i.e.,

$$y(\theta) = Cd_{pg} = d_{pg}(1, \theta),$$
$$u(\theta) = \overline{T}_w(\theta) - \overline{T}_{ws}, \qquad (42)$$

where $C(\cdot) = \int_0^1 \delta(\bar{z} - 1)(\cdot)d\bar{z}$ and $\overline{T}_{ws} = T_{ws}/T_o = 1$. Since coagulation is the main mechanism that affects the size of the aerosol particles, we take advantage of the fact that coagulation is negligible below 1500 K, to control the coagulation by varying the process temperature. It was verified through open-loop simulations that the process model with the above manipulated input and controlled output is minimum phase. Therefore, the model of Equation (34) was used as the basis for the synthesis of a nonlinear controller utilizing the control method described in the previous subsection. For this model, $\overline{\sigma}$ was found to be equal to 2 and the necessary output feedback controller was synthesized using the formula of Equation (41) with $y_{sp} - Ch(w)$ replaced by $y_{sp} - Ch(x)$. The tuning parameters of the controller were chosen as $\gamma_1 = 50$ and $\gamma_2 = 400$ to enforce a slightly underdamped response in the closed-loop system. Owing to the stability of the open-loop process, the observer gain, P, was set identically equal to 0.

Several simulation runs were performed to evaluate the disturbance rejection and set-point tracking capabilities of the nonlinear controller, as well as its robustness with respect to uncertainty in model parameters and unmodeled actuator dynamics. In all simulation runs, the aerosol reactor was initially assumed to be at steady-state.

In the first set of simulation runs, we tested the ability of the controller to maintain the reactor at the operating steady-state in the presence of three parallel disturbances: one in the inlet feed temperature (ramp decrease up to -5% of steady-state value in 20 s, constant at -5% until 30 s, ramp increase to -2.5% in the next

20 s and constant thereafter), the second in the inlet mole fraction of $TiCl_4$ (ramp decrease up to -5% of steady-state value in 20 s, constant at -5% until 30 s, ramp increase to -2.5% in the next 20 s and constant thereafter), and the third in the inlet volumetric flow rate (ramp decrease up to -5% of steady-state value in 20 s, constant at -5% until 30 s, ramp increase to -2.5% in the next 20 s and constant thereafter). The resulting closed-loop output (top plot-dashed line) and manipulated input profiles are shown in Figure 4; the open-loop output profile (top plot-solid line) under the disturbances is also shown for comparison. One can clearly see that there is an offset (deviation of the d_{pg} at the steady-state from the set-point value) in the case of open-loop operation (uncontrolled process), while when feedback control is implemented on the reactor one can see that this offset has been eliminated. Note that the controller achieves this attenuation of the effect of disturbances without using any measurements of the disturbances. Regarding complete elimination of the effect of disturbances on d_{pg} at the exit of the reactor, we note that this is not possible to be achieved by any control algorithm; this is due to the fact that these disturbances propagate rapidly through the reactor, owing to the very small residence time of the reactor, about 1 s, and affect the process outlet before any control actuator (mechanism with which the wall temperature is adjusted) with realistic limits can react. In the second set of simulation runs, we tested the ability of the controller to maintain the reactor at the operating steady state in the presence of three disturbances in series: one in the inlet feed temperature (ramp decrease up to -5% of steady-state value from 0 to 10 s, constant from 10 to 20 s, ramp increase to -2.5% in the next 10 s and constant thereafter), the second in the inlet mole fraction of $TiCl_4$ (ramp decrease up to -5% of steady-state value from 20 to 30 s, constant at -5% from 30 to 40 s, ramp increase to -2.5% in the next 10 s and constant thereafter), and the third in the inlet volumetric flow rate (ramp decrease up to -5% of steady-state value from 40 to 50 s, constant at -5% from 50 to 60 s, ramp increase to -2.5% in the next 10 s and constant thereafter). Figure 5 shows the open-loop output (top plot-solid line), closed-loop output (top plot-dashed line), and manipulated input profiles. Again the controller performs very well regulating the output at the steady-state value, after an initial transient period. From these two simulation runs, it is evident that even though the very small residence time of the reactor and the natural limits on the response of the control actuator do not allow completely eliminating the effect of disturbances on d_{pg} for all times, the use of feedback control helps to attenuate, and eventually eliminate, the effect of disturbances and significantly improve process performance compared to open-loop operation.

In the next simulation run, we tested the set-point tracking capabilities of the controller for a 10% increase in the set-point value of d_{pg} at the exit of the reactor which was imposed at $t = 0$ s. Figure 6 shows the profiles of the controlled output and manipulated input. It is clear that the nonlinear controller smoothly derives the controlled output to the new set-point value, while requesting a smooth control action which is physically realizable (i.e., the rate of change of the wall temperature is less than 2 K per s).

Finally, we tested the robustness of the controller with respect to parametric model uncertainty and unmodeled actuator dynamics. In both simulation runs, a 10% increase in the set-point value of d_{pg} at the exit of the reactor was imposed at $t = 0$ s. Figure 7 shows the closed-loop output and

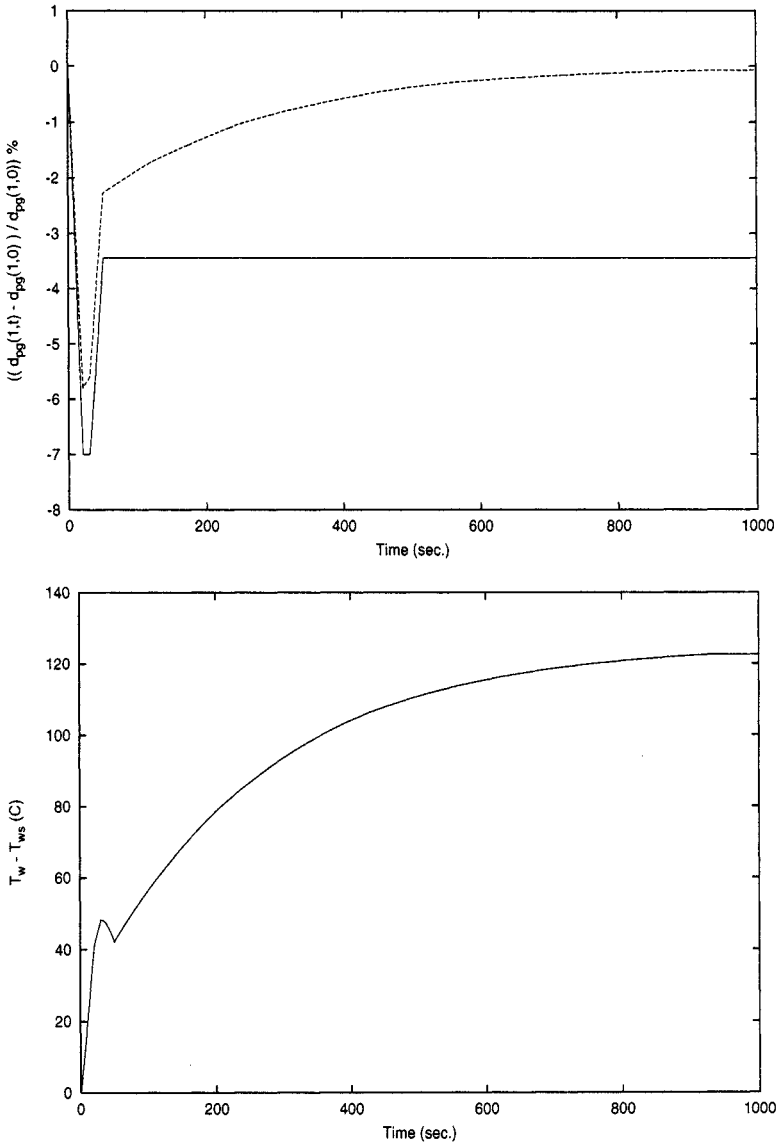

FIGURE 4. Open-loop profile (solid line) and closed-loop profile (dashed line) of $((d_{pg}(1,t) - d_{pg}(1,0)) / (d_{pg}(1,0)))\%$ and manipulated input profile under nonlinear control. Parallel disturbances in inlet flow rate, temperature of inlet stream, and inlet precursor mole fraction.

manipulated input profiles in the presence of 5% constant modeling errors in the parameters A, B, and E. Again, the nonlinear controller exhibits very good robustness properties, driving the output to its new set point. To test the robustness with respect to unmodeled actuator dynamics, the process model of Equations (26)–(33) was augmented with the following dynamical system, which represents the actuator dy-

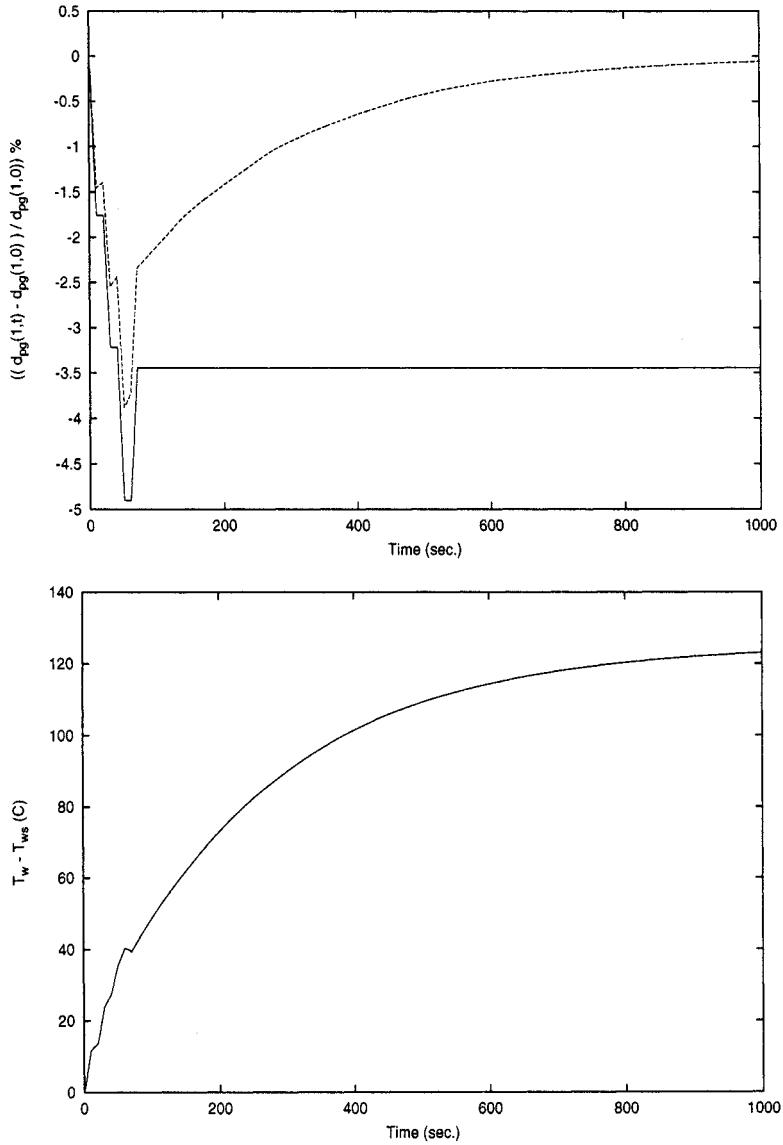

FIGURE 5. Open-loop profile (solid line) and closed-loop profile (dashed line) of $((d_{pg}(1,t) - d_{pg}(1,0)) / (d_{pg}(1,0)))\%$ and manipulated input profile under nonlinear control. Disturbances in series in inlet flow rate, temperature of inlet stream, and inlet precursor mole fraction.

namics, $\varepsilon_z \dot{z}_1 = -z_1 + z_2$, $\varepsilon_z \dot{z}_2 = -z_2 + u$, where $z_1, z_2 \in \mathbb{R}$ are actuator states, z_1 is the actuator output, and ε_z is a small parameter characterizing how fast the actuator dynamics are. When $\varepsilon_z = 0.05$, we found that the nonlinear controller regulates successfully the closed-loop output to its new set-point value exhibiting very good robustness with respect to unmodeled dynamics; the closed-loop output and manipulated in-

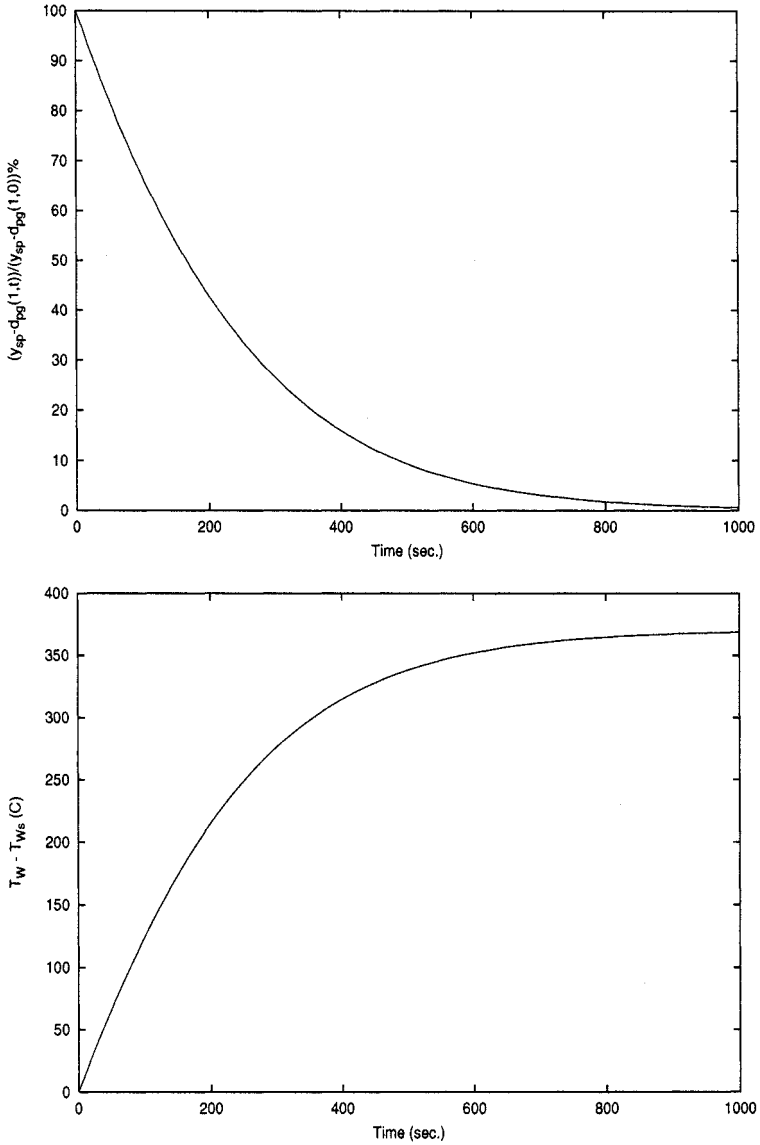

FIGURE 6. Closed-loop profile of $((y_{sp} - d_{pg}(1,t)) / (y_{sp} - d_{pg}(1,0)))\%$ and manipulated input profile under nonlinear control. Nominal conditions-set-point change.

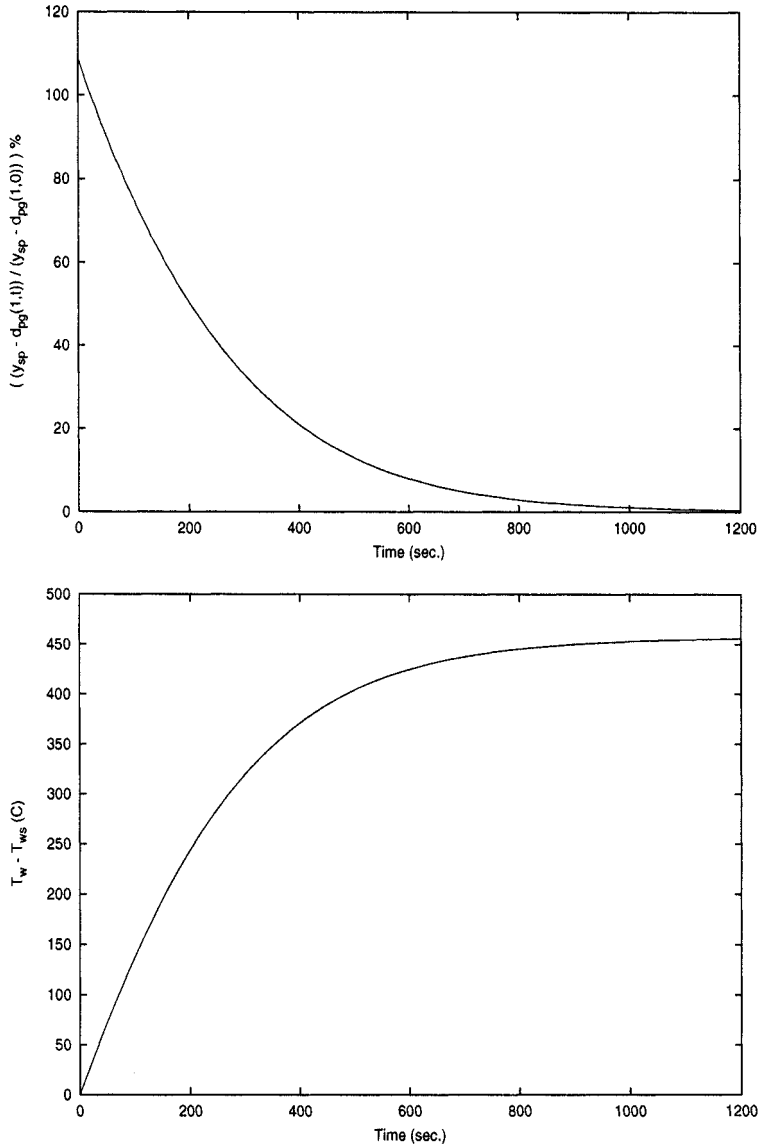

FIGURE 7. Closed-loop profile of $((y_{sp} - d_{pg}(1,t)) / (y_{sp} - d_{pg}(1,0)))\%$ and manipulated input profile under nonlinear control. Parametric uncertainty-set-point change.

put profiles for this simulation run are, as expected, almost identical to the ones shown in Figure 6, and therefore they will be omitted for brevity.

REMARK 8: Regarding the practical implementation of the nonlinear output feedback controller, we note that the wall temperature, $\overline{T}_w$, cannot be manipulated directly but indirectly through manipulation of the furnace temperature. To this end, a controller should be designed based on an ODE model that describes the furnace dynamics, and should operate in an internal loop to manipulate the electrical power supply or fuel flow rate (depending on the type of furnace used) to ensure that the furnace temperature obtains the values computed by the distributed controller. Of course, when such a controller is used, a slight deterioration of the closed-loop response obtained under the assumption that $\overline{T}_w$ can be manipulated directly will occur.

CONCLUSIONS

In this work, we studied the modeling and control of an aerosol flow reactor used to produce titania powder by gas phase oxidation of titanium tetrachloride. Initially, a fundamental mathematical model was derived for the process which describes the spatio-temporal evolution of the three leading moments of the aerosol volume distribution, as well as the evolution of the concentrations of the species and temperature of the continuous phase. The model accounts for simultaneous nucleation, Brownian and shear-induced coagulation, and convective transport and comprises of eight nonlinear first-order hyperbolic PDEs. The process model was subsequently used to synthesize a nonlinear output feedback controller which manipulates the temperature of the reactor wall to achieve an aerosol size distribution in the outlet of the reactor with desired geometric average particle diameter. The performance and robustness of the nonlinear controller were successfully tested through computer simulations.

Financial support from a National Science Foundation CAREER award, CTS 9733509, is gratefully acknowledged. The authors would also like to thank S. K. Friedlander for helpful suggestions.

References

Akhtar, M. K., Xiong, Y., and Pratsinis, S. E. (1991). Vapor Synthesis of Titania Powder by Titanium Tetrachloride Oxidation, *AIChE J.* 37:1561–1570.

Bird, R. B., Stewart, E. W., and Lightfoot, E. N. (1960). *Transport Phenomena*, John Wiley & Sons, Inc., New York.

Brock, J. R., Kuhn, P. J., and Zehavi, D. (1986). Condensation Aerosol Formation and Growth in a Laminar Coaxial Jet: Experimental, *J. Aerosol Sci.* 17:11–22.

Chiu, T., and Christofides, P. D. (1999a). Robust Nonlinear Control of a Continuous Crystallizer, *Comp. & Chem. Eng.* 23(s):249–252.

Chiu, T., and Christofides, P. D. (1999b). Nonlinear Control of Particulate Processes, *AIChE J.* 45:1279–1297.

Chiu, T., and Christofides, P. D. (2000). Robust Control of Particulate Processes Using Uncertain Population Balances, *AIChE J.* 46:266–280.

Christofides, P. D., and Daoutidis, P. (1996). Feedback Control of Hyperbolic PDE Systems, *AIChE J.* 42:3063–3086.

Dimitratos, J., Elicabe, G., and Georgakis, C. (1994). Control of Emulsion Polymerization Reactors, *AIChE J.* 40:1993–2021.

Eaton, J. W., and Rawlings, J. B. (1990). Feedback Control of Chemical Processes Using On-line Optimization Techniques, *Comp. & Chem. Engng.* 14:469–479.

Friedlander, S. K. (1977). *Smoke, Dust, and Hase: Fundamentals of Aerosol Behavior*, Wiley, New York.

Friedlander, S. K. (1983). Dynamics of Aerosol Formation by Chemical Reaction, *Annals. N.Y. Acad. Sci.* 83:354–364.

Hashemi, R., and Epstein, M. A. (1982). Observability and Controllability Considerations in Crystallization Process Design, *AIChE Symp. Ser.* 78:81–190.

Hill, P. J., and Ng, K. M. (1996). New Discretization Procedure for the Agglomeration Equation, *AIChE J.* 42:727–741.

Hounslow, M. J., Ryall, R. L., and Marshall, V. R. (1988). A Discretized Population Balance for Nucleation, Growth and Aggregation, *AIChE J.* 34:1821–1832.

Kalani, A., and Christofides, P. D. (1999). Nonlinear Control of Spatially-Inhomogeneous Aerosol Processes, *Chem. Eng. Sci.* 54:2669–2678.

Kelley, K. (1960). *High-Temperature Heat-Content, Heat-Capacity and Entropy Data for the Elements and Inorganic Compounds*, United States Government Printing Office, Washington, D.C.

Kobata, A., Kusakabe, K., and Morooka, S. (1991). Growth and Transformation of TiO_2 Crystallites in Aerosol Reactor, *AIChE J.* 37:347–359.

Kumar, S., and Ramkrishna, D. (1996a). On the Solution of Population Balance Equations by Discretization-I. A Fixed Pivot Technique, *Chem. Eng. Sci.* 51:1311–1332.

Kumar, S., and Ramkrishna, D. (1996b). On the Solution of Population Balance Equations by Discretization-II. A Moving Pivot Technique, *Chem. Eng. Sci.* 51:1333–1342.

Landgrebe, J. D., and Pratsinis, S. E. (1990). A Discrete Sectional Model for Particulate Production by Gas Phase Chemical Reaction and Aerosol Coagulation in the Free Molecular Regime, *J. Coll. Inter. Sci.* 139:63–86.

Lee, K. W., Chen, H., and Gieseke, J. A. (1984). Log-Normally Preserving Size Distribution for Brownian Coagulation in the Free-Molecule Regime, *Aerosol Sci. Tech.* 3:53–62.

Pratsinis, S. E. (1988). Simultaneous Nucleation, Condensation, and Coagulation in Aerosol Reactors, *J. Coll. Inter. Sci.* 124:416–426.

Pratsinis, S. E. (1989). Particle Production by Gas-to-Particle Conversion in Turbulent Flows, *J. Aerosol Sci.* 20:1461–1464.

Pratsinis, S. E., Bai, H., Biswas, P., Frenklach, M., and Mastrangelo, S. V. R. (1990). Kinetics of Titanium [IV] Chloride Oxidation, *J. Am. Ceram. Soc.* 73:2158–2161.

Pratsinis, S. E., and Spicer, P. T. (1998). Competition Between Gas Phase and Surface Oxidation of $TiCl_4$ During Synthesis of TiO_2 Particles, *Chem. Eng. Sci.* 53:1861–1868.

Ramkrishna, D. (1985). The Status of Population Balances, *Rev. Chem. Eng.* 3:49–95.

Rawlings, J. B., and Ray, W. H. (1987a). Emulsion Polymerization Reactor Stability: Simplified Model Analysis, *AIChE J.* 33:1663–1667.

Rawlings, J. B., and Ray, W. H. (1987b). Stability of Continuous Emulsion Polymerization Reactors: a Detailed Model Analysis, *Chem. Eng. Sci.* 42:2767–2777.

Rohani, S., and Bourne, J. R. (1990). Self-Tuning Control of Crystal Size Distribution in a Cooling Batch Crystallizer, *Chem. Eng. Sci.* 12:3457–3466.

Semino, D., and Ray, W. H. (1995). Control of Systems Described by Population Balance Equations-I. Control-lability Analysis, *Chem. Eng. Sci.* 50:1805–1824.

Williams, M. M. R., and Loyalka, S. K. (1991). *Aerosol Science: Theory & Practice*. Pergamon Press, Oxford, England.

Xiong, Y., and Pratsinis, S. E. (1991). Gas Phase Production of Particles in Reactive Turbulent Flows, *J. Aerosol Sci.* 12:637–655.

Received May 19, 1999; accepted October 1, 1999.

APPENDIX

In this section, the derivation of the hyperbolic PDEs describing the evolution of the three leading moments of the aerosol in the free molecule size regime, Equations (16)–(18), is given. The derivation of the moment equations in the continuum size and turbulent size regimes, Equations (19)–(22), is similar and will be omitted for brevity. Substituting the expression for the nucleation rate into the population balance of Equation (2), we obtain

$$\frac{\partial n}{\partial t} = -\frac{\partial (v_z n)}{\partial z} + N_{av} k C_1 \delta(v - v_1) + \frac{1}{2}\int_0^v \beta_{FM}(v-\bar{v}, \bar{v}) n(v-\bar{v}) n(\bar{v})\, d\bar{v} - n(v)\int_0^\infty \beta_{FM}(v, \bar{v}) n(\bar{v})\, d\bar{v}. \quad (43)$$

Zeroth moment: Integrating both sides of the equation over particle volume, making the substitution $v - \bar{v} = y$ in the third term

on the right-hand side and using that $M_0 = \int_0^\infty n(v)dv$, we obtain

$$\frac{\partial M_0}{\partial t} = -\frac{\partial(v_z M_0)}{\partial z} + N_{av}kC_1 + \frac{1}{2}\int_0^\infty\int_0^\infty \beta_{FM}(y,\bar{v})n(y)n(\bar{v})d\bar{v}dy - \int_0^\infty\int_0^\infty \beta_{FM}(v,\bar{v})n(v)n(\bar{v})d\bar{v}dv. \quad (44)$$

The collision frequency function for the free molecule regime, β_{FM}, given in Equation (6) can be written as

$$\beta_{FM}(v,\bar{v}) = B_1 b_0 (v^{-\frac{1}{2}} + \bar{v}^{-\frac{1}{2}})(v^{\frac{1}{3}} + \bar{v}^{\frac{1}{3}})^2. \quad (45)$$

Writing y as v, substituting the expression for β_{FM} in Equation (44), and using Equation (15), we get

$$\frac{\partial M_0}{\partial t} = -\frac{\partial(v_z M_0)}{\partial z} + N_{av}kC_1 - \frac{B_1 b_0}{2}\int_0^\infty \Big(M_0 v^{\frac{1}{6}} + 2M_{1/3}v^{-\frac{1}{6}} + M_{2/3}v^{-\frac{1}{2}} + M_{-1/2}v^{\frac{2}{3}} + 2M_{-1/6}v^{\frac{1}{3}} + M_{1/6}\Big)n(v)dv. \quad (46)$$

Using again Equation (15), we finally obtain

$$\frac{\partial M_0}{\partial t} = -\frac{\partial(v_z M_0)}{\partial z} + N_{av}kC_1 - B_1 b_0 (M_{2/3}M_{-1/2} + 2M_{1/3}M_{-1/6} + M_{1/6}M_0). \quad (47)$$

First moment: Multiplying both sides of Equation (43) by v, integrating over all particle volume and using that $M_1 = \int_0^\infty vn(v)dv$, we obtain

$$\frac{\partial M_1}{\partial t} = -\frac{\partial(v_z M_1)}{\partial z} + N_{av}kC_1 v_1. \quad (48)$$

Second moment: Multiplying both sides of Equation (43) by v^2 and performing calculations similar to the case for the zeroth moment (with coefficient b_2 used as b_0 in the expression of β_{FM}), we obtain

$$\frac{\partial M_2}{\partial t} = -\frac{\partial(v_z M_2)}{\partial z} + N_{av}kC_1 v_1^2 + 2b_2 B_1 (M_{5/3}M_{1/2} + 2M_{4/3}M_{5/6} + M_{7/6}M_1). \quad (49)$$